The scramblases VMP1 and TMEM41b are required for primitive endoderm specification by targeting WNT signaling

Markus Holzner1, Tea Sonicki1, Hugo Hunn1, Vamshidhar R. Gade2, Karsten Weis2, Anton Wutz1#, and Giulio Di Minin1#

1 Institute of Molecular Health Sciences, Department of Biology, ETH Zurich, Zurich, Switzerland
2 Institute of Biochemistry, Department of Biology, ETH Zurich, Zurich, Switzerland

corresponding authors: awutz@ethaz.ch (AW); giulio.diminin@biol.ethz.ch (GDM)

ABSTRACT

The VMP1 and TMEM41b ER resident proteins share a DedA domain, which defines their lipid scramblase activity. Loss of either gene results in embryonic lethality in mice, and defects in autophagy and lipid droplet metabolism. To understand their role in pluripotency and specification, we generated Vmp1 and Tmem41b mutant mouse Embryonic Stem Cells (ESCs). We observe that ESCs carrying mutations in Vmp1 and Tmem41b are viable, proliferate normally, and conserve a largely intact pluripotency-associated transcriptional profile. Despite clear defects in the accumulation of LC3-positive autophagosomes and lipid droplets, ESCs carrying combined mutations in Vmp1 and Tmem41b can differentiate into a wide range of embryonic cell types. However, we find that simultaneous loss of Vmp1 and Tmem41b impairs the specification of primitive endoderm-like cells. We observe a delayed differentiation of mutant ESCs into extra-embryonic stem (XEN) cells. Mechanistically, we discover that mutant cells upregulate DDIT3, a WNT inhibitor. Chemical stimulation of the WNT cascade can rescue the differentiation delay. Our findings reveal a redundant function of the lipid scramblases VMP1 and TMEM41b and identify a specific role in cell signaling during extraembryonic endoderm development.

INTRODUCTION

The role of vesicle trafficking and membrane lipid composition becomes increasingly important to understand cell signaling. Recently, the role of lipid scramblases has been implicated in viral infection, such as in the severe acute respiratory syndrome coronavirus 2 (SARS-CoV-2) (Baggen et al., 2021; Hoffmann et al., 2021; Kratzel et al., 2021; Sun et al., 2021; Trimarco et al., 2021), cancer development (Folkerts et al., 2019; Gilabert et al., 2013; Guo et al., 2012; Lin et al., 2021; Rodriguez et al., 2017; Ropolo et al., 2020), and inflammatory diseases (Jiang et al., 2022; Li et al., 2023b; Loncle et al., 2016; Yao et al., 2023; Zack et al., 2023). The vacuole membrane protein 1 (VMP1) and transmembrane protein 41B (TMEM41B) are two lipid scramblases that share a highly conserved DedA domain (Ghanbarpour et al., 2021; Li et al., 2021). They localize at the ER membrane and are distinguished from other ER-associated flippases or scramblases by the property to facilitate bi-directional lipid diffusion in an ATP- and Ca2+-independent manner. Vmp1 and Tmem41b activities are necessary for autophagosome formation (Molejon et al., 2013; Moretti et al., 2018), lipid droplet metabolism (Li et al., 2021; Morishita et al., 2019), and lipoprotein formation (Hama et al., 2022). Additional reports proposed a more global role in vesicle transport (Bard et al., 2006) and ER protein homeostasis (Tornero-Ecija et al., 2022). Despite their multifaceted functions, the absence of these factors does not appear to impact cell survival significantly. Compensatory mechanisms shared by VMP1 and TMEM41b or between other ER scramblases might be involved in maintaining cellular homeostasis. A systematic comparison between the activities of Vmp1 and Tmem41b has not yet been performed. VMP1 depletion leads to pronounced defects in autophagosome assembly (Molejon et al., 2013; Moretti et al., 2018), while TMEM41B appears to play a pivotal role in maintaining lipid droplet homeostasis and serves as a crucial factor in RNA virus replication (Hoffmann et al., 2021; Huang et al., 2021).

VMP1 and TMEM41B are both essential in embryonic development. Vmp1 (Morishita et al., 2019) and Tmem41b (Van Alstyne et al., 2018) deficient mice die around E8.5 because of severe developmental delay and impaired implantation. Prior studies formulated a hypothesis where Vmp1 restricts the transfer of vital nutrients to the embryo by blocking the synthesis and release of lipoproteins from the visceral endoderm. However, the observation that mice with a deficiency in crucial genes for

lipoprotein biogenesis, such as ApoB and Mttp, experience mortality at later stages (specifically, E10.5) (Farese et al., 1995; Raabe et al., 1998), implies a distinct and earlier involvement of VMP1 and TMEM41B in embryo development.

During implantation, the mouse embryo is composed by three distinct lineages: the trophectoderm, responsible for placental development; the primitive endoderm (PE), contributing to yolk sac formation; and the epiblast (EPI), primed to develop into the embryo itself (Arnold and Robertson, 2009). The EPI and PE are specified within the inner cell mass (ICM) at the blastocyst stage. Defects in the formation of these lineages are challenging to characterize *in vivo* due to their occurrence in a pre-implantation stage and the small size of the embryo. To investigate the role of VMP1 and TMEM41B in early-embryo linage specification, we studied the ability of mutant cells to differentiate *in vitro* towards embryonic germ layers. We found that a combined mutation of Vmp1 and Tmem41b in ESCs results in a specific defect in PE formation and a delayed conversion to Extra-embryonic endoderm cells (XEN). We find that this delay can be rescued by activation of WNT signaling.

RESULTS

Vmp1 and Tmem41b knockout ESCs show accumulation of LC3+ autophagosome and lipid droplets

To assess the influence of Vmp1 and Tmem41b depletion on mouse ESCs and in early embryo development, we generated independent knockout clones by introducing genomic deletions via the CRISPR/Cas9 system. A mutation of the Vmp1 gene was achieved by introducing an indel in Exon 2 (Fig.1A). This strategy aims to preserve the expression of miR-21, which overlaps with the 3' end of Vmp1 coding sequence (Wang et al., 2020). Edited clones were validated by WB (Fig.S1A). To abrogate Tmem41b expression, we targeted intron 1 and 3, for removing the second and third exons (Fig.1A), which encode the first transmembrane domain of the protein, compromising its correct topology. Additionally, splicing of exon 1 to exon 4 results in a frameshift, suggesting a strong or null allele. The deletion was confirmed on the genomic DNA (Fig.S1B) and mRNA levels by RT-qPCR (Fig.S1C-D). Vmp1 and Tmem41b depleted ESCs show similar morphology (Fig.1B), proliferation (Fig.S1E), and expression of pluripotency markers (Fig.S1F-G) compared to WT ESCs. We confirmed that the pluripotent network was unchanged by a transcriptomic analysis performed in Vmp1

100 and Tmem41b mutant cells. Interestingly, this analysis also show that the transcription
101 profile of cells was marginally affected by the depletion of the two factors (Fig.S1I-J
102 and Table S2).
103 To verify the effect of the mutations on autophagy, we assessed the
104 accumulation of LC3+ autophagosomes. We found an increase of LC3+ puncta in both
105 mutant conditions compared to WT ESCs (Fig.1C and Fig.S2A-B). Interestingly, the
106 increase in the frequency of LC3+ puncta was similar in Vmp1 (4X) and Tmem41b
107 (3,5X) depleted cells. Next, mutant cells were analyzed for the retention of lipid
108 droplets (LD). To amplify LDs, we treated all samples with oleic acid (OA) and
109 visualized LDs by BODIPY staining. Compared to WT ESCs, we observed increased
110 LDs in both mutant conditions (Fig.1D and Fig.S2D). This result was more evident
111 after OA treatment, where Vmp1 and Tme41b mutations led to an increase of 4 times
112 of LD frequency with respect to WT cells. The results suggest that both Vmp1 and
113 Tmem41b are equally necessary for autophagosome and lipid droplet metabolism in
114 ESCs.
115
116 **Vmp1 and Tmem41b are not required for ESC survival and self-renewal**
117 To characterize potential compensatory mechanisms between Vmp1 and Tmem41b,
118 we generated cell lines in which both proteins are depleted. For this purpose, we
119 started with Vmp1 KO ESCs and deleted Tmem41b following the strategy detailed
120 above (Double KO) (Fig.S1A-D). As previously shown in the context of the single
121 mutants, Double KO cells show no differences in ESC morphology (Fig.S1H) and
122 proliferation (Fig.S1E). To further characterize mutant ESCs, we analyzed secretory
123 compartments. The morphology of ER, Golgi apparatus, and Late Endosomes
124 (Fig.S3A) is unaffected in all mutant cells. In line with these findings, the transcription
125 profile of Double KO cells showed a limited perturbation in gene expression (Fig.1E).
126 Simultaneous depletion of both Vmp1 and Tmem41b does not result in a greater
127 number of differentially regulated genes compared to Vmp1 KO cells (Fig.1F). Minimal
128 overlap of differentially expressed genes was detected among mutant cell lines (Fig.1F
129 and Fig.S3B), and we did not observe enrichment for genes that are involved in
130 defined cellular processes (Fig.1G, Fig.S3C-D). The pluripotency network, as also
131 shown by IF staining (Fig.S1F-G), was not perturbed by the simultaneous absence of
132 Vmp1 and Tmem41b. We concluded that Vmp1 and Tmem41b are not necessary for
133 maintaining ESC homeostasis.

134

135 **Vmp1 and Tmem41b have redundant functions**

136 We found that Double KO cell lines show an exacerbated phenotype in
137 autophagosome and LD accumulation in respect to single mutants. In the Double KO,
138 we did not detect an additional increase in the number of autophagosomes per cell
139 (Fig.1H and Fig.S2A-B). However, comparing their size distribution, we found about
140 14% of LC3 clusters of the Double KO to be of larger size (>3μm), compared to the
141 8% of autophagosomes across the single mutations and 3% in the WT condition (Fig.1I
142 and Fig.S2C). The simultaneous depletion of Vmp1 and Tmem41b had a greater
143 impact on LD formation. Double KO cells show a high enrichment of LDs in the
144 absence of oleic acid treatment, which was instead necessary to visualize LDs in WT
145 and single mutant cells (Fig.1J and Fig.S2D-E). Considering that the used stain could
146 also dye lipid-containing compartments like autophagosomes (O'Rourke et al., 2009),
147 we confirmed enriched lipid droplets in Double KO cells with refractive index
148 tomography, a labelling-independent technique (Fig.1K and Fig.S2F-G). Together,
149 these results indicate that Vmp1 and Tmem41b share redundant functions, as the
150 depletion of both genes exacerbates autophagosome and lipid droplet accumulation.

151

152 **Loss of VMP1 and TMEM41b affects ESC potential to differentiate into primitive**
153 **endoderm**

154 To assess the effect of Vmp1 and Tmem41b on the differentiation potential of ESCs,
155 we used embryoid body (EB) differentiation (Fig.2A). Vmp1, Tmem41b, and double
156 mutant ESCs formed well-defined EBs that resembled those of WT cells. We
157 evaluated variations in the differentiation potential of mutant cells by comparing gene
158 expression by RT-qPCR. For each mutant, the differentiation potential of two
159 independent clones was tested. After 6 days, genes expressed in ectoderm (Sox1 and
160 Fgf5), mesoderm (Actc1 and Brachyury) and endoderm (Gata6 and Dab2) are
161 upregulated during the process of differentiation (Fig.2B and Fig.S4A), while the
162 expression of pluripotent markers (Nanog and Pou5f1) was lost (Fig.2B and Fig.S4A).
163 All cell lines analyzed efficiently differentiated into ectoderm and mesoderm lineages
164 (Fig.2C and Fig.S4B-C). Notably, Double KO EBs showed a decreased expression of
165 the endoderm markers Dab2 (100%) and Gata6 (42% of experiments) (Fig.2C and
166 Fig.S4C). Neither single mutant showed Dab2 downregulation even if a decreased
167 endoderm specification was detected, as shown by Gata6 expression levels in

168 experiments performed with Vmp1^{KO} (45%) and Tmem41b^{KO} (40%) cells (Fig.2C and
169 Fig.S4C). Our results indicate that combined mutation of Vmp1 and Tmem41b leads
170 to abrogated Dab2 expression and predisposes variability in the expression of other
171 endodermal genes.

172 We confirmed the ability of Double KO cells to differentiate into ectodermal
173 lineages by generating SOX1-positive spinal cord organoids (Fig.S4D). Mesodermal
174 differentiation was inferred by the ability of double mutant EBs to form contractile
175 cardiomyocytes after plating on gelatin-coated dishes (Video S1-2). We subsequently
176 performed immunostaining on sections of day 6 EBs to evaluate the protein expression
177 and distribution of several endoderm markers. Expression of GATA4, GATA6, and
178 SOX17 was detected but noticeably decreased in Double KO compared to WT EBs
179 (Fig.2D-E). Loss of GATA4 and GATA6 staining was pronounced at the border of the
180 EBs, which resembles the primitive endoderm layer (Zeevaert et al., 2020). In line with
181 these findings, we confirmed the absence of DAB2 in Double KO EBs (Fig.2F). Dab2
182 is mainly expressed In the primitive endoderm, while the other markers are known to
183 be expressed in both primitive and definitive endoderm.

184 The significant reduction in both mRNA and protein levels of Dab2, along with
185 the weakened expression of endoderm markers at the edges of embryoid bodies,
186 provides evidence that the absence of Vmp1 and Tmem41b results in a particular
187 deficiency in the formation of primitive endoderm.

188

189 **Vmp1 and Tmem41b mutations delay ESC differentiation into Extra Embryonic**
190 **Stem Cells (XEN)**

191 To further characterize endodermal differentiation, we examined the impact of
192 depleting Vmp1 and Tmem41b on extra-embryonic stem (XEN) cell specification. XEN
193 cells resemble the primitive endoderm (PE) of the blastocyst and allow to recapitulate
194 *in vitro* the signaling and transcriptional program activated during PE specification
195 (Kruithof-de Julio et al., 2011). Double KO and WT cells were differentiated into XEN
196 cells upon treatment with Activin A and Retinoic Acid (Niakan et al., 2013). After 6 days,
197 we observed that the majority (>80%) of ESCs differentiated to XEN clusters
198 presenting stellate and refractile morphology (Niakan et al., 2013) in the WT sample
199 (Fig.3A). In Double KO cells, the formation of these clusters was strongly impaired.
200 We confirmed XEN identity and the Double KO defect by analyzing the expression of
201 XEN markers by RT-qPCR (Fig.S5A) and immunostaining (Fig.3B and Fig.S5B). It is

worth noting that the small number of derived XEN cells from Double KO ESCs can be expanded for multiple passages, as shown in Fig. S5C. This result suggests that the absence of Vmp1 and Tmem41b does not completely prevent XEN specification but causes a delayed entry into XEN differentiation.

Lack of WNT signal in Vmp1 and Tmem41b mutant cells impairs XEN specification

To chracterize the effect of Vmp1 and Tmem41b depletion on XEN specification, we analyzed the transcription profile of Double KO and WT cells during the differentiation process. We performed RNA sequencing on cells on the second day of differentiation to identify differences in gene expression. Already at this time point, the expression of XEN-dependent genes (Ngondo et al., 2018) was strongly down-regulated in Double KO cells (Fig.3C-D and Fig.5E). At the transcriptional level, depletion of Vmp1 and Tmem41b did not significantly impact processes involving lipid metabolism, autophagy, or ER maintenance (Fig.S5D).

During the XEN differentiation process, we observed specific deregulation of genes related to the WNT pathway in Double KO cells (Fig.3E-F). A close analysis of WNT pathway-deregulated genes allowed to identify several well-established WNT-target genes, such as Frzb, Sox17, Wnt3, and Ccdnd1 (Du et al., 2009; Tetsu and McCormick, 1999; Zhang et al., 2009). Their down-regulation strongly suggests a decrease in activity of the WNT pathway in mutant cells which is a plausible explanation for the XEN specification defects (Athanasouli et al., 2023). Interestingly, we detected Ddit3 among the upregulated genes in Double KO cells. DDIT3 is an inhibitor of the WNT signaling by repressing the transcriptional activity of the TCF7/TCF4 complex (Chiu et al., 2019). We confirmed higher level of DDIT3 protein in Double KO cells (Fig.4A), and quantified a fourfold increase over WT cells (Fig.4B).

To investigate if XEN differentiation of double mutant cells can be rescued by WNT signaling, we chemically activated WNT signaling. We used a GSK kinase inhibitor (CHIR) as a WNT agonist. GSK inhibition did not affect XEN specification in wild-type ESCs. However, WNT activation significantly enhanced the formation of XEN cells in double mutant ESCs (as shown in Fig. 3D-F and Fig. S5B). Collectively, our data indicate how Vmp1 and Tmem41b affect WNT signaling, and explain the delay detected during primitive endoderm specification.

236 **DISCUSSION**

237 Vmp1 and Tmem41b have been recently identified in genetic screens designed to
238 study a variety of cellular processes, such as autophagy, lipid metabolism, virus
239 maturation, pathway modulation, and ER stress. The pleiotropic function and peculiar
240 structure of the DedA domain have prompted multiple studies addressing its mode of
241 action and role in cellular homeostasis. An important point under evaluation is whether
242 Vmp1 and Tmem41b work cooperatively or show specialization for different cellular
243 processes. By deriving ESCs lacking the expression of Vmp1 and Tmem41b, we
244 reported that their absence has a similar effect on autophagy and lipid droplet
245 accumulation. Moreover, we show that simultaneous depletion of both genes
246 exacerbate single mutant defects, particularly in the context of LD formation. Our
247 findings support the existence of a partial redundancy between Vmp1 and Tmem41b
248 activity. It would be tempting to speculate that variable expression levels could account
249 for the contrasting cell dependencies observed across different cellular systems. While
250 Tmem41b's transcriptional regulation is still largely unknown, Vmp1 expression is
251 known to be influenced by external stimuli (Lo Re et al., 2012; Wang et al., 2020).

252 We find that ESCs can self-renew and maintain a substantial differentiation
253 potential independent of TMEM41B and VMP1. Double knockout cells differentiate
254 efficiently into lineages of the three germ layers despite severe defects in autophagy
255 and lipid droplet metabolism (Mizushima and Levine, 2010). It would be interesting to
256 further investigate how the lipid composition equilibrium between the inner and outer
257 leaflets of ER membranes is maintained in the absence of Vmp1 and Tmem41b. Other
258 ER-resident scramblases are Ca2+ dependent, proposing that compensation of Vmp1
259 and Tmem41b absence might require an increased energy status and/or could trigger
260 supplementary signaling events.

261 We verified that ESCs lacking Vmp1 and Tmem41b show a strong delay in the
262 differentiation of extraembryonic (XEN) stem cells *in vitro*. Embryoid body experiments
263 further support defective primitive endoderm specification, which may account for the
264 embryonic lethality observed in Vmp1 and Tmem41b KO embryos (Morishita et al.,
265 2019; Van Alstyne et al., 2018). More permissive growth conditions may explain the
266 requirement for simultaneous depletion of both genes *in vitro*, while the absence of
267 one factor is sufficient to cause the primitive endoderm delay in embryos. Defects in
268 endoderm specification were also observed in Embryoid bodies derived from single
269 Vmp1^{KO} or Tmem41b^{KO} cells but with lower consistency than those derived from

Double KO cells. The finding of WNT signaling deregulation in Vmp1 and Tmem41b XEN cells, explains the specification delay detected in mutant cells: it has been shown that WNT/TCF7L1 transcriptional response is necessary *in vitro* and *in vivo* to promote PE expansion (Athanasouli et al., 2023). Retardation – not impairment – of PE specification induced by Vmp1 or Tmem41b mutations might still lead to embryo implantation but also to the accumulation of defects, which are incompatible with the gastrulation stage.

The direct dependence of the embryo's phenotype on defects on autophagy or lipid/lipoprotein distribution is unlikely. Both KO embryos die at day E8.5 with severe signs of developmental delay, which is already evident at E7.5. Mutant mice with defects in autophagy or LD metabolism either reach the pup stage in the former case (Kuma et al., 2017) or at least die at E10.5 after proper gastrulation and during organogenesis (Farese et al., 1995; Raabe et al., 1998). We propose that PE defects in Vmp1/Tmem41b depleted cells are caused by the increased activity of the WNT repressor DDIT3 which we show to be stabilized at the transcriptional and protein level in KO cells (Fig.4F). DDIT3 is activated via the PERK/ATF4 pathway by ER stress (Rozpedek et al., 2016) or Calcium-dependent mechanisms upon Vmp1 depletion in the absence of ER stress (Li et al., 2023a). Notably, downstream activation of the WNT cascade through chemicals fully rescues the defects of Vmp1 and Tmem41b mutant cells during XEN specification. Thereby, this study presents novel evidence illustrating the roles of Vmp1 and Tmem41b in acting at the interface of cell homeostasis and signaling modulation, adding to their scramblase activity the potential to modulate developmental processes.

MATERIALS AND METHODS

Cell Culture

Mouse ES cells were maintained as previously described in chemically defined 2i medium with added leukemia inhibitory factor (LIF) as described in Di Minin et al. (Di Minin et al., 2022). Base media composition: DMEM (Gibco, #41965039), 15% FBS (Biowest, #S1810-500) 1% sodium pyruvate (Gibco, 11360-070), 1% non-essential amino acids (Gibco, #11140-035). Lif (2000 U/mL, homemade), PD0325901 (1 μM, AxonMedchem, #391210-10-9) and Chiron (3 μM, AxonMedchem, #252917-06-9) are added fresh before use.

304

305 **EB differentiation**

306 To obtain embryonic bodies (EBs), 200k ESCs were plated on Day1 in ESCs base
307 media without 2i and LIF (see cell culture) into a well of a Sphericalplate5D
308 (Kugelmeiers). On Day4, EBs have formed and are transferred to a pHEMA coated
309 6cm culture dish and cultured until Day6. EBs are then collected and subjected to RNA
310 extraction and RT-qPCR analysis or prepared for sectioning and immunofluorescence.
311 In brief, EBs are fixed in 4% PFA for 30 min, cryoprotected in 10%, 20% and 30%
312 sucrose and then embedded and frozen in Tissue Freezing Medium (Leica,
313 #14020108926). 15 µm sections were prepared on a cryotome, mounted onto
314 Superfrost Plus Adhesion slides (VWR international GmBH, #631-0108) and
315 processed for immunofluorescence staining.

316

317 **Cardiomyocyte differentiation**

318 EBs were formed as previously described. On Day4, EBs were collected and seeded
319 onto a non-treated 10cm dish, maintaining ESC base media. Cardiomyocytes
320 randomly specified and were observed as early as on Day6 of differentiation.

321

322 **Spinal Cord Organoids (SCOs) formation**

323 For derivation of SCOs, ESCs were plated in EBs media (DMEM- F12 (Gibco) and
324 Neurobasal Medium (Gibco) (1:1 ratio) supplemented with 200 mM L-glutamine and
325 10% of Knockout serum replacement) on Sphericalplate 5D dishes (Kugelmeiers AG).
326 On day 2, SCOs were transferred in 10 cm tissue culture dishes and treated with RA
327 (10 nM). SCOs were collected and processed for analysis at day 5.

328

329 **Xen Differentiation**

330 XEN cells were obtained following a protocol by Niakan et al. with minor changes
331 (Niakan et al., 2013). In brief, 230k cells were plated in XEN medium on a gelatin-
332 coated 3cm dish. The next day, the media was replaced with Xen medium containing
333 0.1 µM retinoic acid (Thermo Fischer, #17110052) and 10 ng/mL Activin A (Peprotech,
334 #120-14). On Day4, the medium was again replaced by XEN medium, no further
335 supplements were added, and on Day6 samples were either analyzed by IF or qPCR.
336 Rescue of double KO Xen differentiation was performed by adding 1 µM Chiron
337 (AxonMedchem, #252917-06-9) at Day2, together with the retinoic acid and Activin A.

338 Media was changed on day 4 to Xen medium. XEN medium composition: RPMI 1640
339 (Gibco, #61870010), GlutaMAX^{TM} (Gibco, #61870036), 15% FBS (Biowest, #S1810-
340 500), 0,1 mM ß-mercaptoethanol (Sigma, #BCCB9882).
341
342 **CRISPR-Cas9 editing to generate mutant ESC lines**
343 Vmp1: the gRNA (gagacgcatagcaatgagta) was cloned into a px330 vector (Addgene,
344 #158973). Per 3cm well, 300k ESCs were plated and transfected with 2.5 µg of gRNA
345 containing plasmid, as well as 0.25 µg of a GFP expressing plasmid (pCMV-GFP).
346 GFP-positive cells were enriched by FACS and plated as single cells. Colonies were
347 picked. Analysis by WB was used to identify identified VMP1 KO lines. Tmem41b: the
348 gRNAs (gtatgtttgacctgggcgaa and gagtgacatgtggaaatcag) were cloned into px330
349 vectors, and KO clones were derived as described above. PCR analysis of the edited
350 locus (FW: atcttggacagggggagttc RV: gaccaggggttcattgtcatt and FW:
351 cagcacacacctttaatccagc RV: gccacatagcaagcttaagagc) identified KO clones. qPCR of
352 mRNA from Exon 2 (edited locus, N-terminal end) and Exon 7 (C-terminal end) further
353 confirmed the absence of mRNA.
354
355 **Proliferation assay**
356 100k ESCs were plated in a well of a MW12. 48h later, cells were collected and
357 counted. Proliferation rates were calculated as relative factor of cells collected over
358 cells seeded.
359
360 **LC3 staining and size characterization**
361 100k cells were plated on cover-slips, pre-treated with Matrigel (Corning, # 354277),
362 in N2B27 media. N2B27 composition: 50 mL Neurobasal media (Gibco, # 2348949),
363 50 mL Advanced DMEM F12 (Gibco, # 12634010), 4% BSA (Gibco, # 15260), 1% L-
364 Glutamine (Gibco, # 25030024), 1% B27 supplement (Gibco, # 2336837), 0,5% N2
365 supplement (Gibco, # 2328253), and 0,1 mM ß-mercapotethanol (Sigma,
366 #BCCB9882). The next day, samples were fixed in 4% PFA for 15 min, washed 3 times
367 with PBS and then treated with ice-cold MeOH for 5 min on RT. The staining was then
368 performed as described below. Quantification was performed with the Fiji plugin
369 TrackMate (Ershov et al., 2022; Tinevez et al., 2017) to automatically detect puncti
370 with a diameter of 1, 2, and 3 microns at a threshold of 600, 200 and 150, respectively.
371 Nuclei were detected at an average size of 15 microns with a threshold of 10. Unique

372 particles were annotated for 5 different frames for each condition and shown as
373 particles per cell. The experiment was repeated 3 times.
374
375 **LD staining and RF microscopy**
376 Samples were plated as for the LC3 staining. For samples treated with oleic acid,
377 200 µM (Sigma-Aldrich, # O1008-1G) were added at plating, over-night. The next day,
378 samples were incubated in 5 µM BODIPY 493/503 (Invitrogen, #D3922) in PBS and
379 subsequently washed 3 times with PBS and fixed in 4 % PFA for 15 min. Samples
380 were then washed, stained with Dapi for 15 min at RT and mounted with Mowiol.
381 Quantification was performed using the Fiji plugin TrackMate (Ershov et al., 2022;
382 Tinevez et al., 2017) detecting droplets of 1, 2, and 3 microns in diameter at a threshold
383 of 900. Nuclei were detected at 10 micron and a threshold of 1.
384 For RF microscopy, 250k cells were plated per well of a 6 well glass bottom plate
385 (Cellvis, # P06-1.5H-N) in N2B27 media. After 36 h samples were treated with 200 µM
386 oleic acid o/n and then with BODIPY for 3 h. Samples were washed 3 times with PBS
387 and maintained in N2B27 for RF microscopy. The imaging was performed on
388 Tomocube HT-X1 instrument at 37C and 5 % CO2. At least 5-8 images were acquired
389 for each condition for each well. The z-stacks were acquired with 1.06 µm slices. Max
390 Intensity projections (MIP) are generated on the Tomostudio 3.3.9. The fluorescence
391 max intensity projections were resized to Refractive index tomograms for comparison.
392 The ROIs from each image were isolated for further analysis. Comdet plugin was used
393 for identifying high refractive index regions. The approximate particle size was 2 pixels
394 and Intensity threshold values were chosen individually for each image to avoid any
395 false positives or negatives.
396
397 **Immunofluorescence**
398 Samples were washed 3 times with PBS, fixed in 4% PFA for 10 min and again washed
399 3 times with PBS. Samples stained for LC3 were then treated for 5 min with 100%
400 MeOH at RT and washed again 3 times with PBS. Samples were then blocked and
401 permeabilized with 10% donkey serum (Jackson Immunoresearch, #017-000-121)
402 and 0,1% Triton X (Thermo Fischer, # HFH10) in PBS for 20 min and incubated with
403 primary antibodies at 4 °C over-night. Oct4 (1:100, Satna Cruz, # sc-5279), Nanog
404 (1:100, Abcam, # ab80892), Sox2 (1:50, R&D Systems #AF2018), Lc3 (1:200, Cell
405 Signalling, # 2775S), Pdi (1:200, Cell Signalling, # 3501S), Rcas1 (1:200, Cell

406 Signalling, # 12290S), Rab7 (1:200, Cell Signaling, # 9367S) Sox1 (1:50, R&D
407 Systems, # AF3369), Sox17 (1:200 R&D Systems, # AF1924-SP), Gata4 (1:100 R&D
408 Systems, # AF1700-SP), Gata6 (1:100 R&D Systems, # AF1700-SP), Dab2 (1:100
409 BD, # 610464). The next day, samples were washed 3 times with 0.1% Triton X in PBS
410 and then incubated with secondary antibodies and Dapi.
411
412 **Western Blot Analysis**
413 Cells were lysed in membrane buffer (150 mM NaCl, 50 mM Tris-HCl pH 7,5, 1 mM 2-
414 mercaptoethanol (Sigma, #M3148) and 1% CHAPS (Sigma, #C3023) in water).
415 Lysates were run on SDS-Page and transferred to nitrocellulose membranes. Bands
416 were detected with the Amersham ECL Prime Western Blotting Detection Reagents
417 (#RPN2232) and captured on Fujifilm Super RX-N films (#47410). Antibodies for Vmp1
418 (Cell Signalling, #12929S) were used at 1:1000 and DDIT3 1:1000 (Cell Signalling,
419 #2895T). Quantification of western blot bands was performed with ImageJ, normalized
420 to HSP90 (Santa Cruz, #sc-101494).
421
422 **RNA extraction and RT qPCR**
423
424 RNA was extracted with the RNeasy Kit (Quiagen, #74104) following the
425 manufacturer's instructions, including the on-column DNA digestion. EB and SCO
426 samples were pre-treated with the QIAshredder (Quiagen, #79656). cDNAs were
427 prepared using the Bio-Rad iScript Reverse Transcription Supermix for RT-qPCR
428 (#1708841). RT qPCR samples were prepared using the KAPPA SYBR R fast (Roche,
429 KK4611). Primer Sequences:
430 Tmem41b Exon2 FW: TGCAGAAGCTGGATCAGCAA, RV:
431 GAGCCTTGGCGTCATCCATA
432 Tmem41b Exon7 FW: GCAGGTAGAGCGTCACAGAG, RV:
433 TGCAGAGTTGTTCCTGCCTT
434 Sdha FW: CGTTATGTGAGGGGTGTGCCTT, RV:
435 CCTTACCAAACCTTGTGTCTGGA
436 Sox1 FW: ACGTAGCCAACGTAGACAC, RV: ATGAGCGTCGTCCCGTGG
437 Fgf5 FW: GCCTGTCCTTGCTCTTCCTCAT, RV: GGAGAAGCTGCGACTGGTGA
438 Actc1 FW: TGTAGGACCGTGTCGAAACC, RV: CGAAACCACACACTGTTACCG

439 Brachyury FW: TCTCTGGTCTGTGAGCAATGGT, RV:
440 TGCGTCAGTGGTGTGTAATGTG
441 Gata6 FW: GAAGCGCGTGCCTTCATC, RV: GTAGTGGTTGTGGTGTGACAGTTG
442 Dab2 FW: TTGATGATGTGCCTGATGCT, RV: TTTGCTTGTGTTGTCCCTGA
443 Sox17 FW: CCCAACACTCCTCCCAAAGTATC, RV:
444 TTCCCTGTCTTGGTTGATTTCT
445
446 **RNA seq**
447 RNA samples were submitted to the Functional Genomics Center in Zurich (FGCZ) for
448 RNA sequencing. The quality of the RNA was determined with a Fragment Analyzer
449 standard sensitivity RNA measurement (SS RNA kit (15 nt), Agilent, Waldbronn,
450 Germany). The measured concentrations (> 50 ng/µl) and RIN (>9.9) values qualified
451 for a Poly-A enrichment strategy in order to generate the sequencing libraries applying
452 the TruSeq mRNA Stranded Library Prep Kit (Illumina, Inc, California, USA). After Poly-
453 A selection using Oligo-dT beads the mRNA was reverse-transcribed into cDNA. The
454 cDNA was fragmented, end-repaired and polyadenylated before ligation of TruSeq UD
455 Indices (IDT, Coralville, Iowa, USA). The quality and quantity of the amplified
456 sequencing libraries were validated using a Fragment Analyzer SS NGS Fragment Kit
457 (1–6000 bp) (Agilent, Waldbronn, Germany). The equimolar pool of samples was
458 spiked into a NovaSeq6000 run targeting 20M reads per sample on a S1 FlowCell
459 (Novaseq S1 Reagent Kit, 100 cycles, Illumina, Inc, California, USA). Reads from
460 RNA-seq were first preprocessed by Trimmomatic (v0.40) (Bolger et al., 2014) to
461 remove low-quality bases and adapters. Then, reads were aligned to mouse genome
462 GRCm38 (release 81 version from Ensembl) using HISAT2 (v2.2.1) (Kim et al., 2019).
463 HTSeq Count (v2.0.2) (Putri et al., 2022) was used to count reads for each gene
464 (Ensembl GRCm38.81), ignoring reads on overlapped regions. Differentially
465 expressed genes were defined by DESeq2 (v1.40.2) (Love et al., 2014). MA plot was
466 generated using custom-made scripts. Genes significantly enriched show a fold
467 change > 1 and FDR (adjusted p-value) < 0.01. The read counts were transformed in
468 RPKM for the heatmap representations of specific genes and pathways. The genes
469 corresponding to germ-layer differentiation markers (including those for embryonic and
470 extra-embryonic endoderm), biological processes, and signaling pathways were
471 obtained through literature mining and the KEGG database (Table S1). The processed

data are available as excel files (Table S2 and Table S3) and raw data have been deposited on NCBI SRA database under the accession: PRJNA1031567

Competing interest

The authors declare no competing interests.

Acknowledgments

We acknowledge the Functional Genomics Center Zurich (FGCZ) for technical support and Sungsik Lee from ScopeM facility for help on the RF microscopy. We thank G.J. Pereira, C. Fimiani, and U. Sutter for their help with reagents. We thank C. Ciaudo, A. Grison, J. Corn, and K. Basler for their helpful discussions. GDM was supported by the ETH Zurich Postdoctoral Fellowship Program as well as the Marie Curie Actions for People COFUND Program. This work was supported by grants from the Swiss National Science Foundation (SNF grants 31003A_152814/1 and 31003A_175643/1).

Author Contributions

Conceptualization: MH, AW and GDM; Data curation: MH, VG and GDM; Formal analysis: MH, TS, HH, VG, and GDM; Funding acquisition: KW, AW and GDM; Investigation: MH, AW and GDM; Methodology: MH, TS, HH, VG, and GDM; Project administration: AW, GDM; Resources: MH, KW, AW and GDM; Supervision: KW, AW and GDM; Validation: MH, GDM; Visualization: MH, VG and GDM; Writing – original draft: MH, AW and GDM; Writing – review & editing: MH, TS, HH, VG, KW, AW and GDM.

REFERENCES

Arnold, S.J., and Robertson, E.J. (2009). Making a commitment: cell lineage allocation and axis patterning in the early mouse embryo. Nat Rev Mol Cell Biol *10*, 91-103.

Athanasouli, P., Balli, M., De Jaime-Soguero, A., Boel, A., Papanikolaou, S., van der Veer, B.K., Janiszewski, A., Vanhessche, T., Francis, A., El Laithy, Y.*, et al.* (2023). The Wnt/TCF7L1 transcriptional repressor axis drives primitive endoderm formation by antagonizing naive and formative pluripotency. Nat Commun *14*, 1210.

Baggen, J., Vanstreels, E., Jansen, S., and Daelemans, D. (2021). Cellular host factors for SARS-CoV-2 infection. Nat Microbiol *6*, 1219-1232.

Bard, F., Casano, L., Mallabiabarrena, A., Wallace, E., Saito, K., Kitayama, H., Guizzunti, G., Hu, Y., Wendler, F., Dasgupta, R.*, et al.* (2006). Functional genomics reveals genes involved in protein secretion and Golgi organization. Nature *439*, 604-607.

Bolger, A.M., Lohse, M., and Usadel, B. (2014). Trimmomatic: a flexible trimmer for Illumina sequence data. Bioinformatics *30*, 2114-2120.

Chiu, C.S., Tsai, C.H., Hsieh, M.S., Tsai, S.C., Jan, Y.J., Lin, W.Y., Lai, D.W., Wu, S.M., Hsing, H.Y., Arbiser, J.L*., et al.* (2019). Exploiting Honokiol-induced ER stress CHOP activation inhibits the growth and metastasis of melanoma by suppressing the MITF and beta-catenin pathways. Cancer Lett *442*, 113-125.

Di Minin, G., Holzner, M., Grison, A., Dumeau, C.E., Chan, W., Monfort, A., Jerome-Majewska, L.A., Roelink, H., and Wutz, A. (2022). TMED2 binding restricts SMO to the ER and Golgi compartments. PLoS Biol *20*, e3001596.

Du, Y.C., Oshima, H., Oguma, K., Kitamura, T., Itadani, H., Fujimura, T., Piao, Y.S., Yoshimoto, T., Minamoto, T., Kotani, H*., et al.* (2009). Induction and down-regulation of Sox17 and its possible roles during the course of gastrointestinal tumorigenesis. Gastroenterology *137*, 1346-1357.

Ershov, D., Phan, M.S., Pylvanainen, J.W., Rigaud, S.U., Le Blanc, L., Charles-Orszag, A., Conway, J.R.W., Laine, R.F., Roy, N.H., Bonazzi, D*., et al.* (2022). TrackMate 7: integrating state-of-the-art segmentation algorithms into tracking pipelines. Nat Methods *19*, 829-832.

Farese, R.V., Jr., Ruland, S.L., Flynn, L.M., Stokowski, R.P., and Young, S.G. (1995). Knockout of the mouse apolipoprotein B gene results in embryonic lethality in homozygotes and protection against diet-induced hypercholesterolemia in heterozygotes. Proc Natl Acad Sci U S A *92*, 1774-1778.

Folkerts, H., Wierenga, A.T., van den Heuvel, F.A., Woldhuis, R.R., Kluit, D.S., Jaques, J., Schuringa, J.J., and Vellenga, E. (2019). Elevated VMP1 expression in acute myeloid leukemia amplifies autophagy and is protective against venetoclax-induced apoptosis. Cell Death Dis *10*, 421.

Ghanbarpour, A., Valverde, D.P., Melia, T.J., and Reinisch, K.M. (2021). A model for a partnership of lipid transfer proteins and scramblases in membrane expansion and organelle biogenesis. Proc Natl Acad Sci U S A *118*.

Gilabert, M., Vaccaro, M.I., Fernandez-Zapico, M.E., Calvo, E.L., Turrini, O., Secq, V., Garcia, S., Moutardier, V., Lomberk, G., Dusetti, N*., et al.* (2013). Novel role of VMP1 as modifier of the pancreatic tumor cell response to chemotherapeutic drugs. J Cell Physiol *228*, 1834-1843.

Guo, L., Yang, L.Y., Fan, C., Chen, G.D., and Wu, F. (2012). Novel roles of Vmp1: inhibition metastasis and proliferation of hepatocellular carcinoma. Cancer Sci *103*, 2110-2119.

Hama, Y., Morishita, H., and Mizushima, N. (2022). Regulation of ER-derived membrane dynamics by the DedA domain-containing proteins VMP1 and TMEM41B. EMBO Rep *23*, e53894.

Hoffmann, H.H., Schneider, W.M., Rozen-Gagnon, K., Miles, L.A., Schuster, F., Razooky, B., Jacobson, E., Wu, X., Yi, S., Rudin, C.M*., et al.* (2021). TMEM41B Is a Pan-flavivirus Host Factor. Cell *184*, 133-148 e120.

Huang, D., Xu, B., Liu, L., Wu, L., Zhu, Y., Ghanbarpour, A., Wang, Y., Chen, F.J., Lyu, J., Hu, Y*., et al.* (2021). TMEM41B acts as an ER scramblase required for lipoprotein biogenesis and lipid homeostasis. Cell Metab *33*, 1655-1670 e1658.

Jiang, X., Fulte, S., Deng, F., Chen, S., Xie, Y., Chao, X., He, X.C., Zhang, Y., Li, T., Li, F*., et al.* (2022). Lack of VMP1 impairs hepatic lipoprotein secretion and promotes non-alcoholic steatohepatitis. J Hepatol *77*, 619-631.

Kim, D., Paggi, J.M., Park, C., Bennett, C., and Salzberg, S.L. (2019). Graph-based genome alignment and genotyping with HISAT2 and HISAT-genotype. Nat Biotechnol *37*, 907-915.

Kratzel, A., Kelly, J.N., V'Kovski, P., Portmann, J., Bruggemann, Y., Todt, D., Ebert, N., Shrestha, N., Plattet, P., Staab-Weijnitz, C.A*., et al.* (2021). A genome-wide CRISPR screen identifies interactors of the autophagy pathway as conserved coronavirus targets. PLoS Biol *19*, e3001490.

Kruithof-de Julio, M., Alvarez, M.J., Galli, A., Chu, J., Price, S.M., Califano, A., and Shen, M.M. (2011). Regulation of extra-embryonic endoderm stem cell differentiation by Nodal and Cripto signaling. Development *138*, 3885-3895.

Kuma, A., Komatsu, M., and Mizushima, N. (2017). Autophagy-monitoring and autophagy-deficient mice. Autophagy *13*, 1619-1628.

Li, T., Zhao, H., Guo, G., Xia, S., and Wang, L. (2023a). VMP1 affects endoplasmic reticulum stress sensitivity via differential modulation of the three unfolded protein response arms. Cell Rep *42*, 112209.

Li, X.Q., Zeng, L., Liang, D.G., Qi, Y.L., Yang, G.Y., Zhong, K., Chu, B.B., and Wang, J. (2023b). TMEM41B Is an Interferon-Stimulated Gene That Promotes Pseudorabies Virus Replication. J Virol *97*, e0041223.

Li, Y.E., Wang, Y., Du, X., Zhang, T., Mak, H.Y., Hancock, S.E., McEwen, H., Pandzic, E., Whan, R.M., Aw, Y.C*., et al.* (2021). TMEM41B and VMP1 are scramblases and regulate the distribution of cholesterol and phosphatidylserine. J Cell Biol *220*.

Lin, W., Sun, Y., Qiu, X., Huang, Q., Kong, L., and Lu, J.J. (2021). VMP1, a novel prognostic biomarker, contributes to glioma development by regulating autophagy. J Neuroinflammation *18*, 165.

Lo Re, A.E., Fernandez-Barrena, M.G., Almada, L.L., Mills, L.D., Elsawa, S.F., Lund, G., Ropolo, A., Molejon, M.I., Vaccaro, M.I., and Fernandez-Zapico, M.E. (2012). Novel AKT1-GLI3-VMP1 pathway mediates KRAS oncogene-induced autophagy in cancer cells. J Biol Chem *287*, 25325-25334.

Loncle, C., Molejon, M.I., Lac, S., Tellechea, J.I., Lomberk, G., Gramatica, L., Fernandez Zapico, M.F., Dusetti, N., Urrutia, R., and Iovanna, J.L. (2016). The pancreatitis-associated protein VMP1, a key regulator of inducible autophagy, promotes Kras(G12D)-mediated pancreatic cancer initiation. Cell Death Dis *7*, e2295.

Love, M.I., Huber, W., and Anders, S. (2014). Moderated estimation of fold change and dispersion for RNA-seq data with DESeq2. Genome Biol *15*, 550.

Mizushima, N., and Levine, B. (2010). Autophagy in mammalian development and differentiation. Nat Cell Biol *12*, 823-830.

Molejon, M.I., Ropolo, A., Re, A.L., Boggio, V., and Vaccaro, M.I. (2013). The VMP1-Beclin 1 interaction regulates autophagy induction. Sci Rep *3*, 1055.

Moretti, F., Bergman, P., Dodgson, S., Marcellin, D., Claerr, I., Goodwin, J.M., DeJesus, R., Kang, Z., Antczak, C., Begue, D.*, et al.* (2018). TMEM41B is a novel regulator of autophagy and lipid mobilization. EMBO Rep *19*.

Morishita, H., Zhao, Y.G., Tamura, N., Nishimura, T., Kanda, Y., Sakamaki, Y., Okazaki, M., Li, D., and Mizushima, N. (2019). A critical role of VMP1 in lipoprotein secretion. Elife *8*.

Ngondo, R.P., Cirera-Salinas, D., Yu, J., Wischnewski, H., Bodak, M., Vandormael-Pournin, S., Geiselmann, A., Wettstein, R., Luitz, J., Cohen-Tannoudji, M.*, et al.* (2018). Argonaute 2 Is Required for Extra-embryonic Endoderm Differentiation of Mouse Embryonic Stem Cells. Stem Cell Reports *10*, 461-476.

Niakan, K.K., Schrode, N., Cho, L.T., and Hadjantonakis, A.K. (2013). Derivation of extraembryonic endoderm stem (XEN) cells from mouse embryos and embryonic stem cells. Nat Protoc *8*, 1028-1041.

O'Rourke, E.J., Soukas, A.A., Carr, C.E., and Ruvkun, G. (2009). C. elegans major fats are stored in vesicles distinct from lysosome-related organelles. Cell Metab *10*, 430-435.

Putri, G.H., Anders, S., Pyl, P.T., Pimanda, J.E., and Zanini, F. (2022). Analysing high-throughput sequencing data in Python with HTSeq 2.0. Bioinformatics *38*, 2943-2945.

Raabe, M., Flynn, L.M., Zlot, C.H., Wong, J.S., Veniant, M.M., Hamilton, R.L., and Young, S.G. (1998). Knockout of the abetalipoproteinemia gene in mice: reduced lipoprotein secretion in heterozygotes and embryonic lethality in homozygotes. Proc Natl Acad Sci U S A *95*, 8686-8691.

Rodriguez, M.E., Catrinacio, C., Ropolo, A., Rivarola, V.A., and Vaccaro, M.I. (2017). A novel HIF-1alpha/VMP1-autophagic pathway induces resistance to photodynamic therapy in colon cancer cells. Photochem Photobiol Sci *16*, 1631-1642.

Ropolo, A., Catrinacio, C., Renna, F.J., Boggio, V., Orquera, T., Gonzalez, C.D., and Vaccaro, M.I. (2020). A Novel E2F1-EP300-VMP1 Pathway Mediates Gemcitabine-Induced Autophagy in Pancreatic Cancer Cells Carrying Oncogenic KRAS. Front Endocrinol (Lausanne) *11*, 411.

Rozpedek, W., Pytel, D., Mucha, B., Leszczynska, H., Diehl, J.A., and Majsterek, I. (2016). The Role of the PERK/eIF2alpha/ATF4/CHOP Signaling Pathway in Tumor Progression During Endoplasmic Reticulum Stress. Curr Mol Med *16*, 533-544.

Sun, L., Zhao, C., Fu, Z., Fu, Y., Su, Z., Li, Y., Zhou, Y., Tan, Y., Li, J., Xiang, Y.*, et al.* (2021). Genome-scale CRISPR screen identifies TMEM41B as a multi-function host factor required for coronavirus replication. PLoS Pathog *17*, e1010113.

Tetsu, O., and McCormick, F. (1999). Beta-catenin regulates expression of cyclin D1 in colon carcinoma cells. Nature *398*, 422-426.

Tinevez, J.Y., Perry, N., Schindelin, J., Hoopes, G.M., Reynolds, G.D., Laplantine, E., Bednarek, S.Y., Shorte, S.L., and Eliceiri, K.W. (2017). TrackMate: An open and extensible platform for single-particle tracking. Methods *115*, 80-90.

Tornero-Ecija, A., Tabara, L.C., Bueno-Arribas, M., Anton-Esteban, L., Navarro-Gomez, C., Sanchez, I., Vincent, O., and Escalante, R. (2022). A Dictyostelium model for BPAN disease reveals a functional relationship between the WDR45/WIPI4 homolog Wdr45l and Vmp1 in the regulation of autophagy-associated PtdIns3P and ER stress. Autophagy *18*, 661-677.

Trimarco, J.D., Heaton, B.E., Chaparian, R.R., Burke, K.N., Binder, R.A., Gray, G.C., Smith, C.M., Menachery, V.D., and Heaton, N.S. (2021). TMEM41B is a host factor required for the replication of diverse coronaviruses including SARS-CoV-2. PLoS Pathog *17*, e1009599.

Van Alstyne, M., Lotti, F., Dal Mas, A., Area-Gomez, E., and Pellizzoni, L. (2018). Stasimon/Tmem41b localizes to mitochondria-associated ER membranes and is essential for mouse embryonic development. Biochem Biophys Res Commun *506*, 463-470.

Wang, C., Peng, R., Zeng, M., Zhang, Z., Liu, S., Jiang, D., Lu, Y., and Zou, F. (2020). An autoregulatory feedback loop of miR-21/VMP1 is responsible for the abnormal expression of miR-21 in colorectal cancer cells. Cell Death Dis *11*, 1067.

Yao, Y., Gu, J., Li, M., Li, G., Ai, J., and Zhao, L. (2023). WHSC1L1-mediated epigenetic downregulation of VMP1 participates in herpes simplex virus 1 infection-induced mitophagy impairment and neuroinflammation. Mol Immunol *163*, 63-74.

Zack, S.R., Nikolaienko, R., Cook, B., Melki, R., Zima, A.V., and Campbell, E.M. (2023). Vacuole Membrane Protein 1 (VMP1) Restricts NLRP3 Inflammasome Activation by Modulating SERCA Activity and Autophagy. Res Sq.

Zeevaert, K., Elsafi Mabrouk, M.H., Wagner, W., and Goetzke, R. (2020). Cell Mechanics in Embryoid Bodies. Cells *9*.

Zhang, Z., Deb, A., Zhang, Z., Pachori, A., He, W., Guo, J., Pratt, R., and Dzau, V.J. (2009). Secreted frizzled related protein 2 protects cells from apoptosis by blocking the effect of canonical Wnt3a. J Mol Cell Cardiol *46*, 370-377.

630 **FIGURE LEGENDS**

631

632 **Figure 1. Vmp1 and Tmem41b double KO ESCs display increased**
633 **autophagosome and lipid droplet accumulation**

634

635 **(A)** Schematic representation of the CRISPR/Cas9-mediated KO strategy for Vmp1
636 and Tmem41b genes. For depleting Vmp1 (top) a single gRNA inducing an indel
637 mutation has been used. In the case of the Tmem41b gene (bottom), two gRNAs were
638 used to delete exons 2 and 3. The sequences coding for transmembrane domains
639 (TM) are indicated in blue, the conserved DedA domain is highlighted in yellow, red
640 lines indicate cut sites of gRNAs. **(B)** Colony morphology of $VMP1^{KO}$ and $Tmem41^{KO}$
641 ESCs remains unchanged compared to WT ESCs. Scale bar: 100 µm. **(C)** VMP1 and
642 Tmem41b depletion induce accumulation of autophagosomes in ESCs. The graph
643 shows the quantification of LC3 puncta per cell of a representative experiment (see
644 Fig.S2A). Data were collected from more than 200 cells. For each KO condition, two
645 independent clones have been analyzed. Dots correspond to the frames analyzed per
646 sample. Data are represented as mean ± SD **(D)** Vmp1 and Tmem41b depletion leads
647 to the accumulation of lipid droplets (LD) in ESCs. Graph quantifies LD per cell in WT
648 and KO ESCs (see Fig.S2D). ± oleic acid treatment. At least 500 cells were analyzed
649 for every condition; dots represent independent biological replicates. Data are
650 represented as mean ± SD. (**E-G)** Transcriptional analysis of Double KO ESCs did not
651 identify many deregulated genes. **(E)** Shown are differentially regulated genes in
652 Double KO ESCS in blue as MA plot. Genes highlighted in red are pluripotency
653 markers. **(F)** Diagram showing uniquely and collectively differentially expressed genes
654 in Vmp1, Tmem41b, and Double KO ESCs. **(G)** Differentially regulated genes do not
655 cluster in essential processes. The graph shows differentially expressed genes of
656 single and double KO ESCs by cellular processes. Dot size correlates to the number
657 of deregulated genes within a cellular process. **(H-I)** Double KO ESCs accumulate
658 LC3+ autophagosomes of increased size. **(H)** Shown are representative IF images of
659 WT and double KO ESCs stained for LC3. Nuclei are stained with Dapi. Scale bar:
660 20 µm. **(I)** Plotted is the quantification of LC3 puncta of 3 µm in diameter. For each
661 condition, two independent clones have been analyzed. Dots correspond to the frames
662 analyzed per sample. Data were collected from more than 200 cells. Data are
663 represented as mean ± SD. **(J)** Double KO ESCs accumulate LDs without oleic acid

treatment. The number of LDs per cell is plotted for all KO clones. Data are represented as mean ± SD. **(K)** Double KO ESCs present an increased amount of LD visualized through refractive index microscopy (top) and co-stained with BODIPY.

Figure 2. Double KO ESCs specify all germ layers, but not the primitive endoderm

(A) Schematic representation of an Embryonic Body (EB) which consists of 3 different lineages. The ectoderm expresses Fgf5 and Sox1 (grey), the mesoderm Actc1 and Brachyury (blue), and the endoderm by Gata6 and Dab2 (yellow). **(B)** ESCs differentiated to EBs express lineage markers for ectoderm (Fgf5), mesoderm (Brachyury), and endoderm (Gata6). Graphs show mRNA levels of WT EBs normalized to the Sdha gene. Dots represent biological independent experiments. Data are represented as mean ± SD. **(C)** Double KO ESCs specifically show defects in expressing the primitive endoderm marker, Dab2. qPCR analysis for Sox1, Actc1 and Dab2 mRNA expression in mutant EBs relative to WT EBs. Two independent clones were analyzed per cell line. Each dot represents an independent experiment. Data are represented as mean ± SD**.** The line at 0,7 indicates an arbitrary threshold after which successful expression of the marker is considered. **(D-F)** Double mutant EBs show decreased expression of endoderm markers. Immunofluorescence images of EB sections stained for the endoderm markers GATA4 and SOX17 **(D)**, GATA6 **(E)**, DAB2 **(F)**. WT in the top panel, two independent clones for Double KO condition in the center and bottom panel. Nuclei are stained with Dapi. Scale bar: 50 µm.

Figure 3. XEN differentiation in Double KO cells is delayed

(A-B) Double KO ESCs show a delay in XEN differentiation. **(A)** Brightfield images of XEN cells at day 6 of differentiation in WT and in Double KO cells. XEN islands are circled in white in the Double KO condition. Scale bar: 100 µm. **(B)** Immunofluorescence images of day 6 XEN cells stained for SOX17 and GATA4. Nuclei are stained with Dapi, Scale bar: 150 µm. **(C-F)** Transcriptional analysis of XEN cells. **(C)** Differentially expressed genes between Double KO and WT cells at day 2 during XEN specification. XEN markers are labeled in red, differentially expressed genes in blue. **(D-E)** GO-Term analysis of differential expressed genes between Double KO and

698 WT conditions in ESCs and XEN cells in the context of developmental processes **(D)**
699 and signaling pathways **(E)**. Dot size corresponds to differentially regulated genes. **(F)**
700 WNT pathway related genes differentially expressed in Double KO cells. Heatmap
701 shows min to max expression of three biological replicates for WT and Double KO
702 XEN cells.
703
704
705 **Figure 4. Activation of WNT signaling fully rescues the delay of Double KO cells**
706 **in XEN differentiation**
707
708 **(A-B)** VMP1 and Tmem41b depletion promotes increase of DDIT3 protein levels. **(A)**
709 Western Blot analysis of DDIT3 expression in WT and Double KO cells differentiated
710 to XEN cells for 2 days. HSP90 is shown as loading control. **(B)** Quantification of
711 increased DDIT3 protein levels in three biological replicates. Expression relative to WT
712 XEN cell and normalized to respective HSP90 expression. Data are represented as
713 mean ± SD. **(C-E)** Chiron-dependent WNT activation rescues the delay of Double KO
714 XEN differentiation. **(C)** Brightfield images show XEN clusters of double KO XEN cells
715 (highlighted by white lines) with and w/o Chiron treatment. Scale bar: 100 µm. IF
716 staining for SOX17 and GATA4 **(D)** or DAB2 and GATA6 **(E)**; nuclei are stained with
717 Dapi. Scale Bar: 150 µm. **(F)** Schematic overview highlighting the correlation between
718 loss of Vmp1 and Tmem41b and decreased WNT signaling via DDIT3.

Figure1

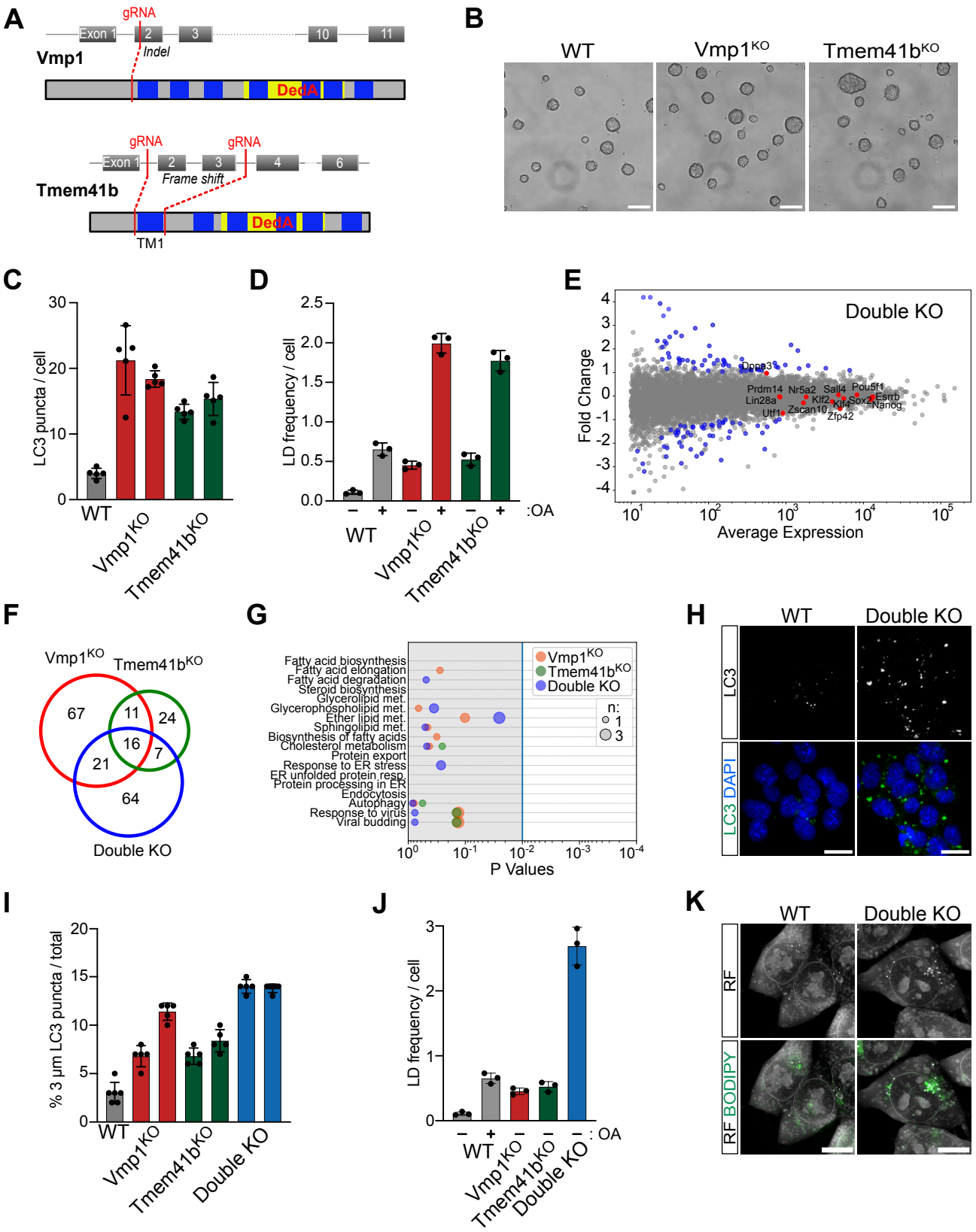
A
gRNA
Exon 1
2
3
10
11
Indel
Vmp1
DedA
gRNA
gRNA
Exon 1
2
3
4
6
Frame shift
Tmem41b
DedA
TM1
B
WT
Vmp1KO
Tmem41bKO
C
LC3 puncta / cell
WT
Vmp1KO
Tmem41bKO
D
LD frequency / cell
:OA
WT
Vmp1KO
Tmem41bKO
E
Double KO
Fold Change
Average Expression
Dppa3
Prdm14
Nr5a2
Sall4
Pou5f1
Lin28a
Klf2
Klf4
Sox2
Esrrb
Nanog
Utf1
Zscan10
Zfp42
F
Vmp1KO
Tmem41bKO
67
11
24
16
7
21
64
Double KO
G
Fatty acid biosynthesis
Fatty acid elongation
Fatty acid degradation
Steroid biosynthesis
Glycerolipid met.
Glycerophospholipid met.
Ether lipid met.
Sphingolipid met.
Biosynthesis of fatty acids
Cholesterol metabolism
Protein export
Response to ER stress
ER unfolded protein resp.
Protein processing in ER
Endocytosis
Autophagy
Response to virus
Viral budding
Vmp1KO
Tmem41bKO
Double KO
n:
1
3
P Values
H
WT
Double KO
LC3
LC3 DAPI
I
% 3 µm LC3 puncta / total
WT
Vmp1KO
Tmem41bKO
Double KO
J
LD frequency / cell
: OA
WT
Vmp1KO
Tmem41bKO
Double KO
K
WT
Double KO
RF
RF BODIPY

Figure 2

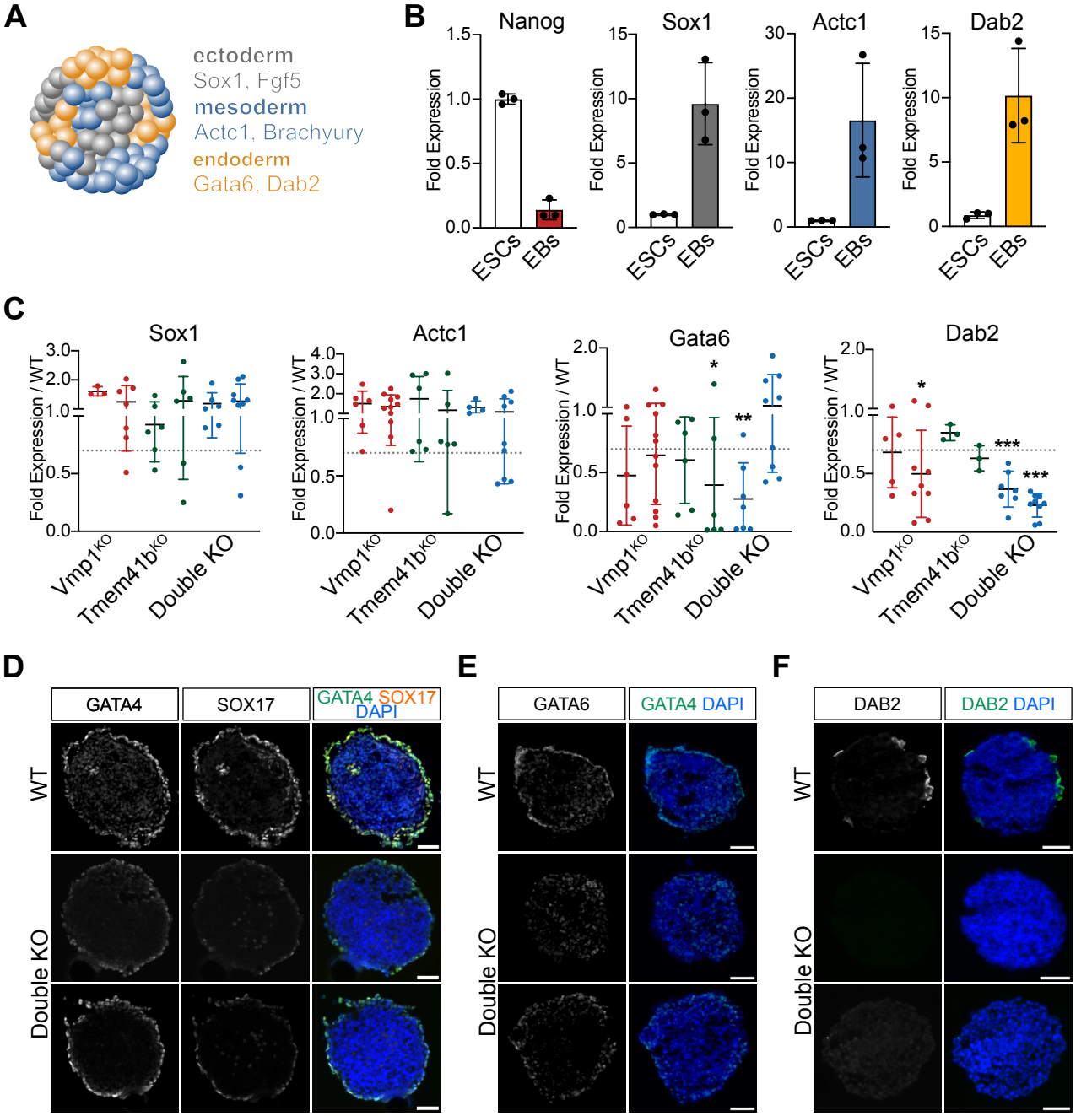
A
ectoderm
Sox1, Fgf5
mesoderm
Actc1, Brachyury
endoderm
Gata6, Dab2
B
Nanog
Sox1
Actc1
Dab2
Fold Expression
ESCs
EBs
C
Sox1
Actc1
Gata6
Dab2
Fold Expression / WT
Vmp1KO
Tmem41bKO
Double KO
D
GATA4
SOX17
GATA4 SOX17 DAPI
WT
Double KO
E
GATA6
GATA4 DAPI
F
DAB2
DAB2 DAPI

Figure 3

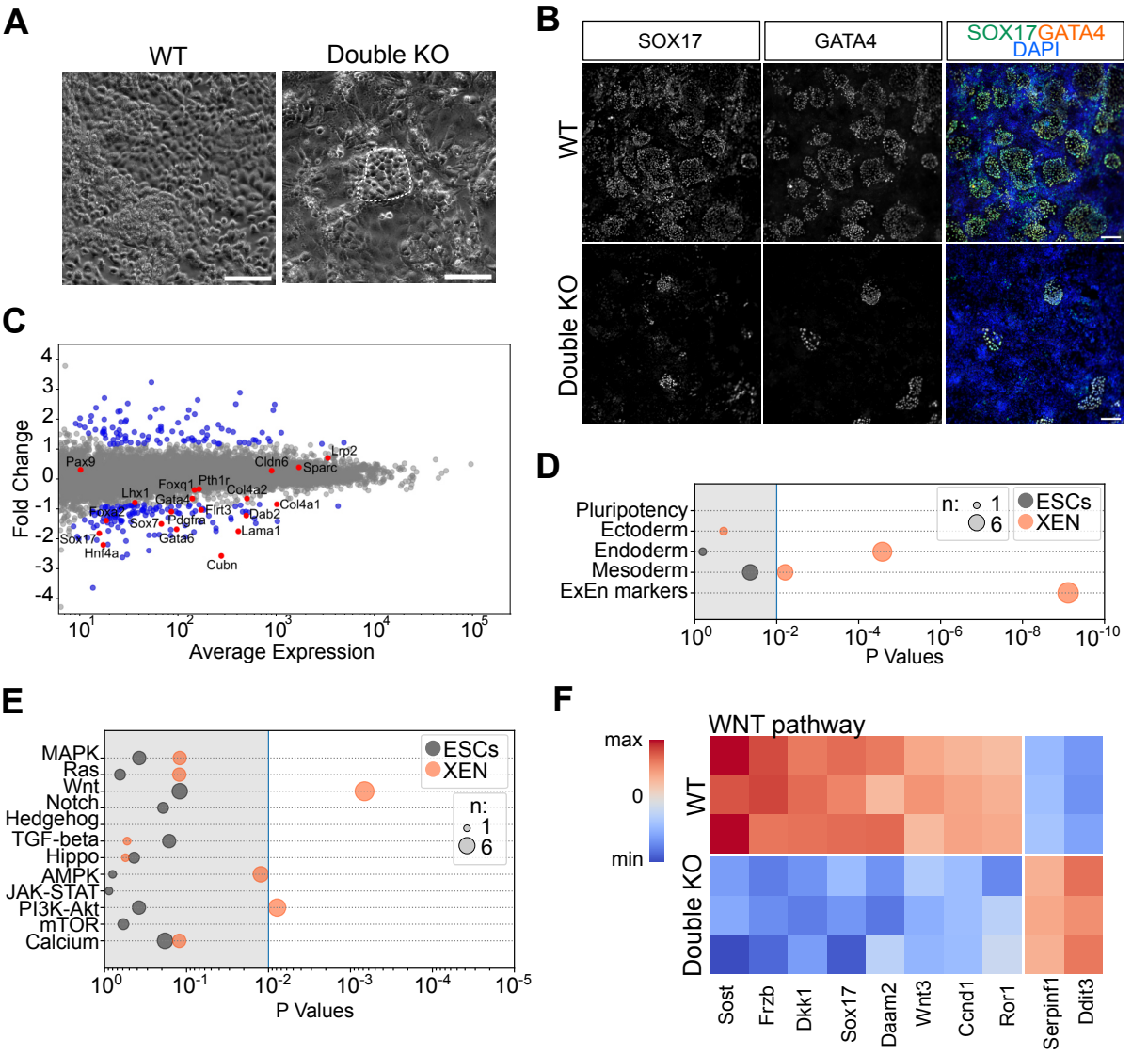
A
WT
Double KO
B
SOX17
GATA4
SOX17GATA4
DAPI
WT
Double KO
C
Fold Change
Average Expression
Pax9
Lrp2
Cldn6
Sparc
Foxq1
Pth1r
Col4a2
Lhx1
Gata4
Col4a1
Elf3
Dab2
Sox7
Pdgfra
Lama1
Sox17
Gata6
Hnf4a
Cubn
D
Pluripotency
Ectoderm
Endoderm
Mesoderm
ExEn markers
P Values
n:
1
6
ESCs
XEN
E
MAPK
Ras
Wnt
Notch
Hedgehog
TGF-beta
Hippo
AMPK
JAK-STAT
PI3K-Akt
mTOR
Calcium
P Values
ESCs
XEN
n:
1
6
F
WNT pathway
max
0
min
WT
Double KO
Sost
Frzb
Dkk1
Sox17
Daam2
Wnt3
Ccnd1
Ror1
Serpinf1
Ddit3

Figure 4

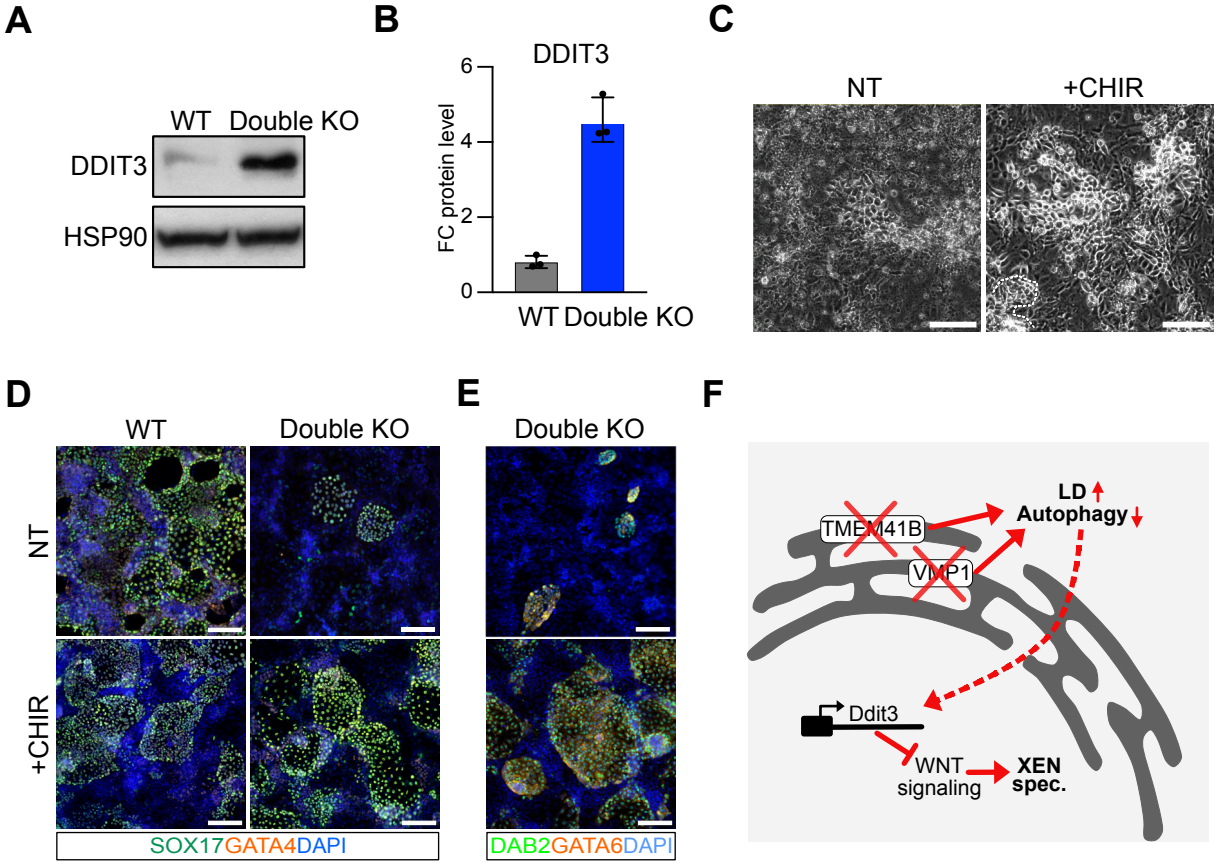
A
WT
Double KO
DDIT3
HSP90
B
DDIT3
FC protein level
6
4
2
0
WT
Double KO
C
NT
+CHIR
D
WT
Double KO
NT
+CHIR
SOX17GATA4DAPI
E
Double KO
DAB2GATA6DAPI
F
TMEM41B
VMP1
LD
Autophagy
Ddit3
WNT
signaling
XEN
spec.